# Ion Trap Networking: Cold, Fast, and Small*

D. L. Moehring,† M. Acton, B. B. Blinov, K.-A. Brickman, L. Deslauriers, P. C. Haljan, W. K. Hensinger, D. Hucul, R. N. Kohn, Jr., P. J. Lee, M. J. Madsen, P. Maunz, S. Olmschenk, D. Stick, M. Yeo, and C. Monroe
*FOCUS Center and University of Michigan, Department of Physics, USA*

J. A. Rabchuk
*Western Illinois University, Department of Physics, USA*

A large-scale ion trap quantum computer will require low-noise entanglement schemes and methods for networking ions between different regions. We report work on both fronts, with the entanglement of two trapped cadmium ions following a phase-insensitive Molmer-Sorensen quantum gate, the entanglement between a single ion and a single photon, and the development of advanced ion traps at the micrometer scale, including the first ion trap integrated on a semiconductor chip. We additionally report progress on the interaction of ultrafast resonant laser pulses with cold trapped ions. This includes fast Rabi oscillations on optical S-P transitions and broadband laser cooling, where the pulse laser bandwidth is much larger than the atomic linewidth. With these fast laser pulses, we also have developed a new method for precision measurement of excited state lifetimes.

## ION ENTANGLEMENT

### Local ion entanglement

Laser-addressed trapped ions with qubits embedded in long-lived internal hyperfine levels hold significant advantages for quantum information applications [1, 2]. A critical issue is the robust generation of scalable entanglement. Trapped-ion entangling gates mediated by phonons of the collective ion motion are susceptible to various forms of noise - qubit and motional decoherence, impure initial conditions, and technical issues associated with the optical Raman lasers driving the gate [1]. Robust schemes for gates based on spin-dependent forces have been proposed [3–6] and experimentally implemented [7, 8] that, for example, relax the purity requirement on the initial motional state of the ions. We have recently realized a Mølmer-Sørensen entangling gate [3, 7, 9] for pairs of trapped $^{111}Cd^+$ ions using an implementation proposed in Refs. 10-11 that reduces sensitivity to optical phase drifts through appropriate Raman beam setup and reduced sensitivity to magnetic field fluctuations through the use of magnetic-field insensitive qubit states. The gate interaction is based on a bichromatic field of first Raman sidebands coupling to a collective vibrational mode of the trapped ions [Fig. 1(a)]. This realizes a nonlinear qubit interaction $H \sim \frac{\hbar\Omega}{2}\sigma_x \otimes \sigma_x$, which can couple $|\downarrow\downarrow\rangle$ to $|\uparrow\uparrow\rangle$ to produce an entangled Bell state $\Psi = \frac{1}{\sqrt{2}}(|\downarrow\downarrow\rangle + |\uparrow\uparrow\rangle)$

A full evaluation of the entangled state including a quantitative measure of the entanglement requires access to the full density matrix, in particular all the off-diagonal coherences. Quantum state tomography [12, 13] is used to reconstruct the density matrix for all four entangled Bell states. Repeated preparation of a target state followed by projective measurements of the two ion-qubits in nine different bases $\{\sigma_i \otimes \sigma_j; i, j = 1, 2, 3\}$ is performed for 200 shots per measurement basis. Maximum likelihood estimation is used to fit the data to a density matrix constrained to a physical form. An example of a reconstructed density matrix for the entangled state $\Psi$ created with the Mølmer-Sørensen scheme is shown in Figure 1(b). The ideal state is created with fidelity ∼0.80. One measure of entanglement that is directly calculable from the density matrix for two qubits is Wooters' entanglement of formation $E$ ranging from zero for a separable state to one for a maximally entangled one [14]. The experimental value for the state in Figure 1(b) is $E$=0.65. The tomographic reconstruction of the entanglement demonstrates universal two-qubit control, which can be directly applied to simple algorithms.

One such algorithm is Grover's searching algorithm which searches an unsorted database quadratically faster than any known classical search [15]. A common analogy is to be given a phone number but no name to go with the number [16]. For $N$ entries in the phone book, the worst case scenario classically requires $N$ queries, and on average requires $N/2$ queries. However, if the correlation between name and phone number is encoded with quantum bits, the name can be found after only about $\sqrt{N}$ queries. The key to the algorithm is in the oracle query which, using entangled superposition, checks if an input state is a solution to the problem. Contingent upon being a solution, the state is marked by flipping the sign of its amplitude. Following the oracle are several quantum operations that amplify the weighting of the marked state independent of which state is marked. After a prescribed number of iterations the marked state accumulates nearly all of the weight and is revealed following a measurement [17]. For $N \gg 1$, the marked element appears with high

*Proceedings of the XVII International Conference on Laser Spectroscopy, edited by E. A. Hinds, A. Ferguson and E. Riis, (World Scientific, Singapore, 2005) 421-428 (2005)

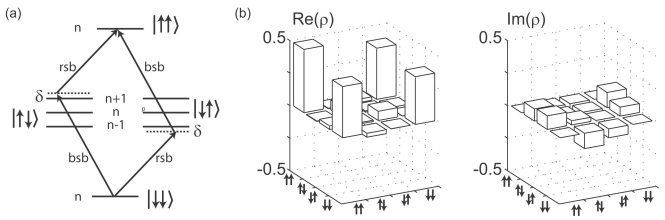


FIG. 1: (a)The Molmer-Sorensen entangling gate is based on a bichromatic field composed of red (rsb) and blue (bsb) Raman sidebands coupling ion spin to collective vibrational levels $\{|n\rangle\}$. Typical gate interaction time to generate the entangled state $\Psi = \frac{1}{\sqrt{2}}(|\uparrow\uparrow\rangle + |\downarrow\downarrow\rangle)$ is 100$\mu$s. (b)Tomographic density matrix reconstruction of the entangled state $\Psi$ created with fidelity ∼0.8.

probability after approximately $\pi\sqrt{N}/4$ iterations, and for the special case of $N = 4$ elements, a single query provides the marked element with unit probability.

Using the Molmer-Sorensen entangling gate described above this algorithm was carried out for a four element search space (n=2 qubits). The algorithm starts by creating an equal superposition of input states with a global single qubit $\pi/2$ rotation. Next the oracle query is applied. This is carried out by first swapping the target marked state, $|xx\rangle$ with the state $|\downarrow\downarrow\rangle$. The Molmer-Sorensen entangling gate is then used in conjunction with single qubit rotations to create a controlled-z gate. This gate takes the $|\downarrow\downarrow\rangle$ state to -$|\downarrow\downarrow\rangle$ and leaves the other states unchanged. Then the $|xx\rangle$ and $|\downarrow\downarrow\rangle$ states are swapped back. This results in the target marked state acquiring a minus sign, $|xx\rangle \rightarrow -|xx\rangle$. Another global single qubit rotation followed by a final entangling gate complete the algorithm by amplifying the weighting of the marked state. Upon measurement the marked state is recovered with 60(2)% probability [18]. The classical counterpart is a simple shell game: suppose a marble is hidden under one of four shells, and after a single query the location of the marble is guessed. Under these conditions the best classical approach gives an average probability of success: $P_{cl} = 1/4 + 3/4(1/3) = 50\%$, (1/4 of the time the query will give the correct location of the marble while 3/4 of the time a guess must be made amongst the three remaining choices with 1/3 probability of choosing the correct location). If Grover's algorithm is used, the answer to the query would always result in a successful 'guess' of the marble's location. Experimentally the marked state was recovered with a probability, averaged over the four markings, of 60(2)%, surpassing the performance of any possible classical search.

### Probabilistic remote ion entanglement

In the ongoing remote ion entanglement experiment, single $^{111}Cd^{+}$ ions are trapped in two different ion traps spaced by approximately one meter. Each ion is initially excited to a state with multiple decay channels and single photons are emitted from each decaying ion. Along a certain emission direction selected by an aperture, each photon's polarization is entangled with particular hyperfine ground states in its de-excited parent ion [19, 20]. Current progress in the entanglement of the ions through joint detection of the photons [21] includes the use of ultrafast laser pulses for single photon generation [Fig. 3(a)] and precise mode-matching of the photons from each ion onto a beamsplitter. Even though the photon emission is a probabilistic process, unlike other probabilistic sources such as two-photon downconversion, this atom-atom entanglement is heralded by the joint detection of the photons, and can be subsequently used for further applications, including scalable quantum computing architectures [22, 23].

## ULTRAFAST LASER INTERACTIONS

### Ultrafast laser cooling

Narrow-band lasers are essential tools for the precise control of internal and external states of cold atoms, from laser cooling of atomic motion to the formation of optical lattices and dipole traps. However, very little has been achieved concerning the control of cold trapped atoms with ultrafast lasers, notwithstanding recent theoretical proposals on ultrafast quantum gates using trapped ions [6, 24]. As a first step toward realization of these proposals, we have observed picosecond Rabi oscillations between the S and P levels of singly ionized cadmium. Additionally, we have directly observed trapped ion laser cooling from broadband pulses [25]. The extent of cooling is determined by directly measuring the spatial localization of the ion within the trap, and the most efficient cooling occurs when the center frequency of the laser is tuned roughly one bandwidth (∼420 GHz) below the atomic resonance. When cooled by the pulsed laser, ions are localized to a few microns corresponding to a temperature of a few Kelvin, allowing clear images of ion crystals even in the face of large amounts of rf micromotion [Fig. 2].

### Precision lifetime measurements

These fast transitions to the excited state have also allowed for a new method for precision lifetime measurements [26]. This method, designed especially to eliminate common systematic errors, involves selective excitation of

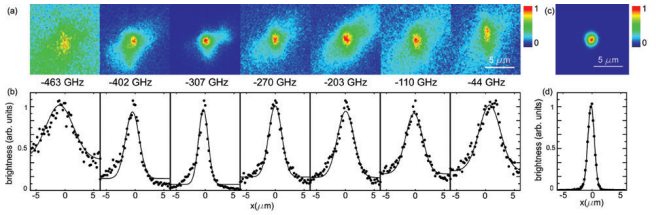


FIG. 2: (a) Images of a single trapped ion taken at various pulsed laser detunings, $\delta/2\pi$, indicated at the bottom. The pulsed laser beam direction in each image is diagonal from lower-left corner to upper-right corner. (b) Crosssections of the images in (a) along the vertical direction. The solid lines are Gaussian fits to the data. (c) An image of a narrow-band laser-cooled ion localized to ∼30 nm, with its crossection and Gaussian fit plotted in (d).

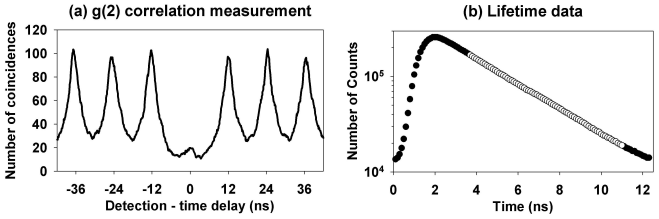


FIG. 3: (a) $g^{(2)}$ correlation function. An absence of a peak at time t=0 (coincident detection) shows that the ion is a single photon source. The peak is not fully extinguished because of background photons scattered off a nearby electrode (as evidenced by the asymmetry in the peak). Between pulses, the curves do not go all the way to zero since the peaks are only 12 ns apart whereas the excited state lifetime is ∼3 ns. (b) Excited state lifetime histogram data for the $5p^2P_{1/2}$ state. The open circles show the data used to extract the excited state lifetime: $3.148 \pm 0.011$ ns.

a single trapped ion to an excited state (lifetime of order nanoseconds) by a fast laser pulse (length of order one picosecond). Arrival of the spontaneously emitted photon from the ion is correlated in time with the excitation pulse, and the distribution of time delays from many such events provides the information for the excited state lifetime. By using this technique, we are able to eliminate prevalent systematic errors such as pulse pileup, radiation trapping, flight from view, sub/superradiance, non-selective excitation and/or detection, and potential effects from applied light during the measurement interval. With uncertainties of less than 0.4%, these results are among the most precise measurements of atomic state lifetimes to date [Fig. 3(b)]. Furthermore, this technique has the potential to achieve ∼ 100 ppm precision by eliminating the remaining technical systematic effects.

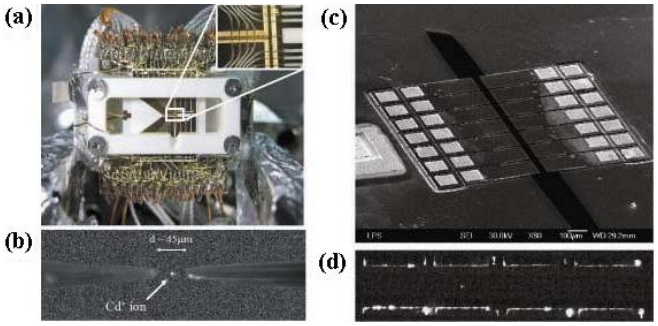


FIG. 4: (a) T-junction trap array. The magnified inset shows the trapping array including the junction. (b) Single Cd+ ion trapped between needles (picture of needle electrodes added to scale). (c) Scanning electron microscope image of monolithic GaAs semiconductor linear ion trap. (d) Image of a single trapped Cd+ ion along a view perpendicular to the chip plane.

## TRAP FABRICATION

### Shuttling ions in two-dimensional arrays

Trapping and shuttling [27–29] trapped ions in complex multi-zone trap structures is critical for scaling the trapped ion quantum computer. We have demonstrated an 11-zone linear ion trap consisting of 49 electrodes in a three-layer geometry, and have shuttled cold $Cd^+$ ions between several zones [Fig. 4(a)]. This trap features a "T"-junction and we have demonstrated reliable shuttling around the corner. Furthermore, we demonstrated controlled swapping of ion positions within a linear crystal by forcing the ions to undergo a "three-point turn" through the junction. This trap topology may be a fundamental building block toward implementing complex entanglement algorithms on an ion trap quantum computer.

### Variable electrode micron-scale needle trap

We report the successful operation of a novel ion trap geometry formed with two needle-like electrodes mounted on linear translation stages, allowing for the trap electrode spacing to be varied in-situ over a range of separations between 20-1000 mm [Fig. 4(b)]. The variable electrodes may allow for the systematic study of a host of ion trap properties at the micron scale, such as electrode surface noise and ion heating. The results of this study may impact the design and construction of future ion trapping apparatus relevant to quantum information applications, and the open geometry of the trap may be suitable for trapped-ion cavity QED.

**Scalable integrated chip trap**

Scaling ion trap quantum computing requires microfabrication methods that allow the production of large scale arrays. We report the successful operation of a micron-scale integrated chip ion trap fabricated from epitaxially-grown GaAs/AlGaAs layers and shaped with chemical and dry etching techniques. Development of this fabrication process may allow scaling elementary ion trap quantum processors to a large number of qubits. Figure 4(c) shows the ion trap and Figure 4(d) shows a single $Cd^+$ ion inside the chip trap.

## ACKNOWLEDGMENTS

This work is supported by the U.S. National Security Agency and Advanced Research and Development Activity under Army Research Office contract and the National Science Foundation ITR program.

† Electronic address: dmoehrin@umich.edu

[1] D. J. Wineland, C. Monroe, W. M. Itano, D. Leibfried, B. E. King, and D. M. Meekhof, *J. Res. Nat. Inst. Stand. Tech.*, **103**, 259 (1998).
[2] B. B. Blinov, D. Leibfried, C. Monroe, and D. J. Wineland, *Quant. Inf. Proc.*, **3(1)**, 1 (2004).
[3] K. Mølmer and A. Sørensen, *Phys. Rev. Lett.*, **82**, 1835 (1999).
[4] E. Solano, R. L. de Matos Filho, and N. Zagury, *Phys. Rev. A*, **59**, R2539 (1999).
[5] G. J. Milburn, S. Schneider, and D. F. V. James, *Fortschr. Phys.*, **48**, 801 (2000).
[6] J. J. Garcia-Ripoll, P. Zoller, and J. I. Cirac, *Phys. Rev. Lett.*, **91**, 157901 (2003).
[7] C. A. Sackett *et al.*, *Nature*, **404**, 256 (2000).
[8] D. Leibfried *et al.*, *Nature*, **422**, 412 (2003).
[9] A. Sørensen and K. Mølmer, *Phys. Rev. A*, **62**, 022311 (2000).
[10] P. C. Haljan, K.-A. Brickman, L. Deslauriers, P. J. Lee, and C. Monroe, *Phys. Rev. Lett.*, **94**, 153602 (2005).
[11] P. J. Lee *et al.*, quant-ph/0505203.
[12] J. B. Altepeter, D. F. V. James, and P. G. Kwiat, *Lecture Notes in Physics*, **649**, 113 (2004).
[13] C. F. Roos *et al.*, *Phys. Rev. Lett.*, **92**, 220402 (2004).
[14] W. K. Wootters, *Phys. Rev. Lett.*, **80**, 2245 (1998).
[15] L. K. Grover, *Phys. Rev. Lett.*, **79**, 325 (1997).
[16] G. Brassard, *Science*, **275**, 627 (1997).
[17] M. Boyer, G. Brassard, P. Høyer, and A. Tapp, *Fortschr. Phys.*, **46**, 493 (1998).
[18] K.-A. Brickman *et al.*, In Preperation.
[19] B. B. Blinov, D. L. Moehring, L.-M. Duan, and C. Monroe, *Nature* **428**, 153 (2004).
[20] D. L. Moehring, M. J. Madsen, B. B. Blinov, and C. Monroe, *Phys. Rev. Lett.* **93**, 090410 (2004).
[21] C. Simon and W. T. M. Irvine, *Phys. Rev. Lett.* **91**, 110405 (2003).
[22] L.-M. Duan, B. B. Blinov, D. L. Moehring, and C. Monroe, *Quantum Inf. Comput.* **4**, 165 (2004).
[23] L.-M. Duan and R. Raussendorf, quant-ph/0502120 (2005).
[24] L.-M. Duan, *Phys. Rev. Lett.* **93**, 100502 (2004).
[25] B. B. Blinov *et al.*, quant-ph/0507074 (2005).
[26] D. L. Moehring *et al.*, *Phys. Rev. A*, **73**, 023413 (2006).
[27] M. D. Barrett *et al.*, *Nature* **429**, 737 (2004).
[28] D. Kielpinski, C. Monroe, and D. J. Wineland, *Nature* **417**, 709 (2002).
[29] M. A. Rowe *et al.*, *Quantum Inf. Comput.* **2**, 257 (2002).